2019 IEEE International Conference on Manipulation, Manufacturing and Measurement on the Nanoscale (3M-NANO)
4-8 August, Zhenjiang

Geometrical Patterns Based Cross-scale Image Registration for AFM and Optical Microscopy

Ziqi Hu, Zhi Fan, Cunhuan Liu, Yinan Wu*, Chao Wang
Institute of Robotics and Automatic Information System
Nankai University
Tianjin, 300350, China
wuyn@nankai.edu.cn

Ziqi Hu, Zhi Fan, Cunhuan Liu, Yinan Wu*, Chao Wang
Tianjin Key Laboratory of Intelligent Robotics
Tianjin, 300350, China
wuyn@nankai.edu.cn

***Abstract*—Image registration is usually used to transform different images from different sensors, times, depths or viewpoints into one coordinate. This paper proposes a novel template matching algorithm based on geometrical patterns, which is proved to be effective in matching AFM and optical images. As for the procedures of the proposed algorithm, firstly the resolution of the AFM image is calibrated as a priori knowledge for image processing in the next few steps. Then, traditional image processing methods, including filtering, binarization and contour-searching, are applied to the raw images sequentially. Centroids of every pattern made up of edges are connected to extract the geometrical feature information of the image. In the end, a designed assessment function is applied to the whole image to calculate each point's matching possibility. Experiments show that, compared with traditional methods, the proposed algorithm provides much more reliable matching results in AFM-optical template matching, offering an effective way for cross-scale images registration.**

Keywords—atomic force microscopy, cross-scale image registration, template matching, geometrical patterns

I. INTRODUCTION

The atomic force microscopy (AFM) has been widely employed in nano-science and nano-technology fields [1, 2]. Compared with traditional imaging and operating methods, an AFM is superior in acquiring truly topographies beyond the limitation of the visible spectrum and operating samples in nano-scale. On the other hand, compared with a scanning tunneling microscope, an AFM presents the unique advantages of no requirement for electrical conductivity of the detected samples, nor strict scanning environments. Based on the merits mentioned above, an AFM is believed to have a wider application [3].

Despite so many merits of an AFM, it has a limited view range, which means it usually needs other imaging equipment to provide a wider vision field. A general way is to set up a confocal AFM system with an optical microscope. However, such confocal mode causes many problems in image locating, due to the cross-scale image registration environment, where AFMs are used in nano-scale and optical microscopes are used in micron-scale. In general, it is necessary to figure out the corresponding location of AFM images in the optical view. For instance, it is important to specify which cell or part is scanned, or keep track of the cell in the long run in pharmacological researches.

Template matching techniques are used to find the location of a sub image, called a *template*, inside an image [4]. According to the function of the template matching technique, it is one of the solutions to overcome the difficulties of locating in cross-scale image registration between AFMs and optical microscopes, where an AFM-scanned image can be treated as a template and an optical image as a reference image. In traditional template matching technique, lots of algorithms have been raised in much previous work utilizing grayscale differences of images. For example, J. N. Sarvaiya *et al.* present a method for medical image registration by template matching based on Normalized Cross-Correlation (NCC) using Cauchy-Schwartz inequality [5]. Besides, L. D. Stefano and S. Mattoccia provide a novel fast template matching technique, referred to as bounded partial correlation (BPC) [6]. However, using only grayscale information appears invalid for AFM-optical template matching in some situation, due to the different underlying fundaments of forming images. Therefore, a novel template matching algorithm adapted to the cross-scale environment need to be proposed to solve image registration problems for AFMs and optical microscopes.

Noticing the uneven distribution of scanned samples, this paper proposes a geometrical patterns based template matching algorithm (GPTM) which is adapted to template matching with images from different sensors in some situation. In the circumstance that images are generated from the AFM and the traditional optical microscopy, there are many similarities at edges. In order to take advantage of this character, raw images are binarized to extract the edge information. Patterns made up of the edges build up geometrical features for the image. Each pattern's centroid is calculated out and connected together to form a convex polygon considered as the geometrical feature information. In the end, a designed assessment function is applied to the whole image to calculate each point's matching possibility.

The rest of this paper is organized as follows. In Section II, the underlying differences between AFM and optical microscopy imaging principles are illustrated in detail, and the main drawbacks of the current grayscale-based template matching methods are stated. In Section III, a geometrical patterns based template matching algorithm (GPTM) is put forward. Section IV presents experimental results to demonstrate the superior performance of the presented method. Finally, the conclusions of this paper are drawn in Section V.

II. DIFFERENCE BETWEEN AFM AND OPTICAL MICROSCOPY IN IMAGING PRINCIPLE

When an AFM detects a biological sample, the probe tip is kept a constant distance upon the sample surface and the tiny force between the probe tip and the sample surface is controlled by a feedback mechanism [7, 8]. During the scanning process, the probe tip's position changes following the topography of the sample surface. The laser from the emitter is reflected by the probe tip and then received by the laser detector, generating a variety of voltages which is then compared with the reference voltage. The difference is sent to the digital controller as feedback [9]. The output of the controller is utilized to control the movement of the piezo-scanner, and the image of the sample topography is constructed by analyzing the control and error signals [8].

978-1-7281-0205-4/19/$31.00©2019 IEEE

Thus grayscale values in such image are determined by the topography of sample surface.

Images captured by an optical microscope can be observed from eyepiece or CCD camera. CCD converts images from analog light signals into digital pixels. CCD sensors, upon exposure to light, accumulate electric charges proportional to the light intensity at corresponding locations. A control circuit makes each capacitor pass its charges to its neighbor. The last capacitor dumps its charges into a charge amplifier, which converts the charge into a voltage. By repeating this process, the controlling circuit converts the entire charges in sensors to a sequence of voltages which are then sampled, digitized, and stored in memory to generate an image. In the traditional optical microscopy, CCD camera is exposed to the light which passes through the sample and lens sequentially. Since the distribution of samples is uneven, intensities of lights passing through the sample from different parts are different. Which means, each pixel's grayscale value is determined by the intensity of the light.

Traditional template matching methods tend to find the correlation of grayscale values between the template image and the source image, which appears invalid in AFM-optical circumstance in some situation. In experiments, as shown in Fig. 1, we used a confocal AFM system with an optical microscope, which allows us to capture optical pictures and scan the interested area in such a view at the same time. Meanwhile, it is important to know which area has been scanned in the optical view. However, it is a tough work that only using eyes to figure out which area the AFM scans referring to the template image. Besides, according to the experiment results, we noticed that samples usually have an uneven distribution which forms many particular geometrical patterns marked in Fig. 2, an optical image of Hela cells. Thus, a geometrical patterns based template matching algorithm is proposed which shows robust performance in AFM-optical template matching.

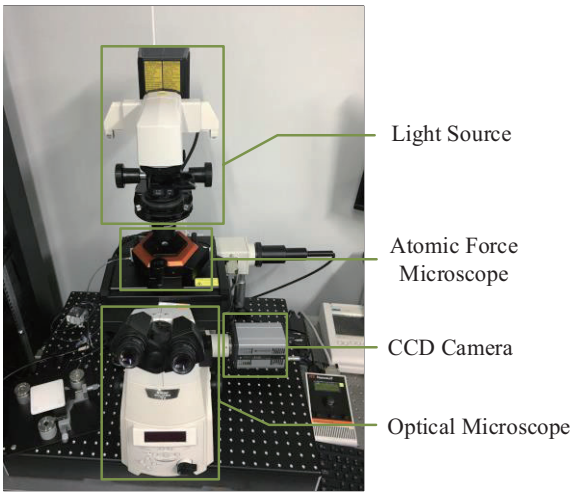

Fig. 1. The confocal AFM system with an optical microscope.

As indicated by the image of the biological samples shown in Fig. 2, the geometrical information provided by samples can be used to apply the similarity algorithm to template matching. Thus geometrical patterns-based template matching algorithm is stated which successfully matches AFM-scanned template images with corresponding areas in the optical source image.

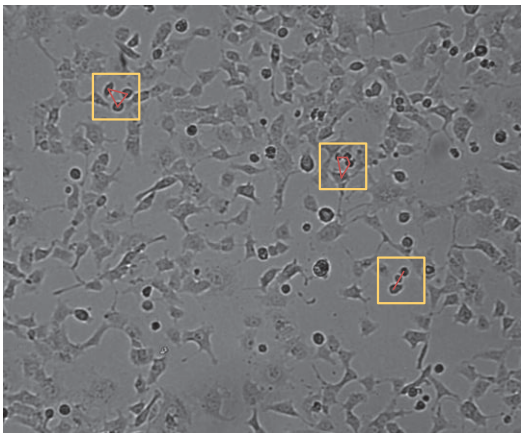

Fig. 2. The optical image of hela cells.

III. Geometrical Patterns Based Template Matching Algorithm Design

A. Calibration and Preprocess

Noticing that an AFM can use the force between the probe tip and petri dish to engrave special patterns on the petri dish's surface, we engraved a square on the surface of a petri dish as shown in Fig. 3. The size of the square is $50\ \mu m \times 50\ \mu m$. The square's size is calibrated in pixel-scale to be 56×56 on 830×700 canvas. Therefore, the transform between AFM scanning size and optical view size is

$$L_x = 113R \cdot W \cdot x\ ,\ L_y = 80R \cdot H \cdot y\ ,$$

where L_x, L_y are width and height in pixel size of AFM-scanned image, R is the magnification of optical microscopy. W and H are the canvas's width and height. The coefficients are validated under 10 times magnification microscopy.

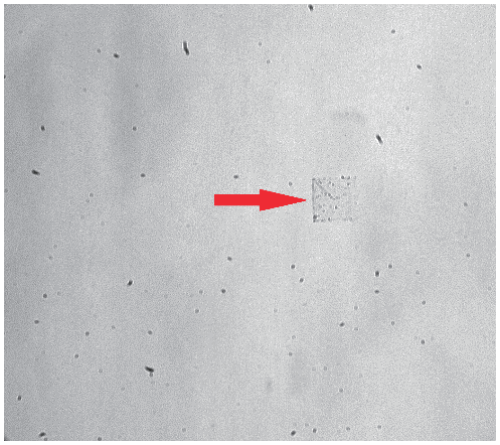

Fig. 3. The square scotch on petri dish's surface (20 ×).

In order to obtain reliable experiment results, a special sample is made by engraving a triangle-shaped pattern onto the petri dish's surface and scanned in size of $60\ \mu m \times 60\ \mu m$ by the AFM as shown in Fig. 4, which would be used to adjust GPTM's parameters in the following steps and other kinds of patterns would be used to prove its effectiveness. Bilateral filtering is used to filter out noises while reserving edge information at the same time. After that, images are transformed into binary images by setting a threshold λ which is defined by

$$\lambda = \frac{\max\{f(x_1, y_1), ..., f(x_n, y_n)\}}{2} + K_1,$$

where $f(x_1, y_1), \ldots, f(x_n, y_n) \in T$, T represents the set of all pixel values of the image, K_1 is the bias parameter.

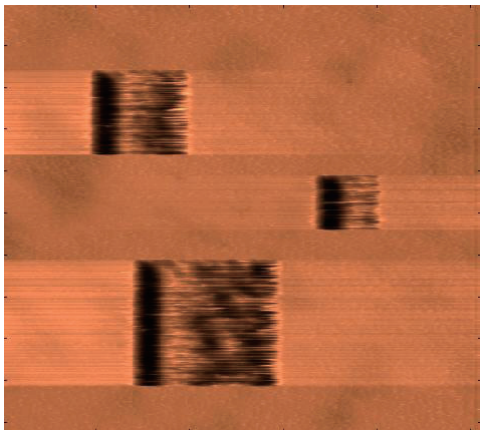

Fig. 4. AFM-scanned sample (triangle-shaped).

As shown in Fig. 5 (a), each pattern's contours can be found to extract the edge information. AFM images and optical images are symmetrical due to the scanning direction. Therefore images are mirror transformed in preprocess. Because of noises, each pattern is claimed to have more than one contour. Small contours are eliminated by setting a threshold K_2 which represents the least length among all contours. Centroid point of each contour is shown in Fig. 5 (b). Canvas is separated into 9 areas, and as for those points located at the same area, centroid point is calculated which is shown in Fig. 5 (c). By connecting them together as shown in Fig. 5 (d), inner corners of the convex polygon are calculated and stacked into the eigenvector

$$\eta = (\cos^{-1}\frac{\vec{a}_1 \cdot \vec{a}_2}{|\vec{a}_1| \cdot |\vec{a}_2|}, ..., \cos^{-1}\frac{\vec{a}_{n-1} \cdot \vec{a}_n}{|\vec{a}_{n-1}| \cdot |\vec{a}_n|}, \cos^{-1}\frac{\vec{a}_n \cdot \vec{a}_1}{|\vec{a}_n| \cdot |\vec{a}_1|})^{\mathrm{T}},$$

where $\vec{a}_1, \ldots, \vec{a}_n$ are all edges of convex polygon. η 's dimensions and 1-norm are used to filter out impossible areas.

B. Calculating each Pattern's Polymerization

By calculating the eigenvector of each pattern, the basic geometrical information of each template image can be extracted out. Among remained possible matching areas, the concept of the polymerization is introduced into assessment function in order to find the precise location of the template image in optical view. Ψ is defined as the set containing all the areas. For each pixel belonging to a specific area, an eigenvector z is defined by its coordinate

$$z = (x, y)^{\mathrm{T}},$$

Ω is the set of feature-pixels in this area, where feature-pixels represent the pixels differing from the background. The covariance matrix C_t for target area t is

$$C_t = \frac{1}{n}\sum_{i=1}^{n}(z_i - \mu)(z_i - \mu)^{\mathrm{T}}, \ t = 1, 2, ..., 9,$$

where

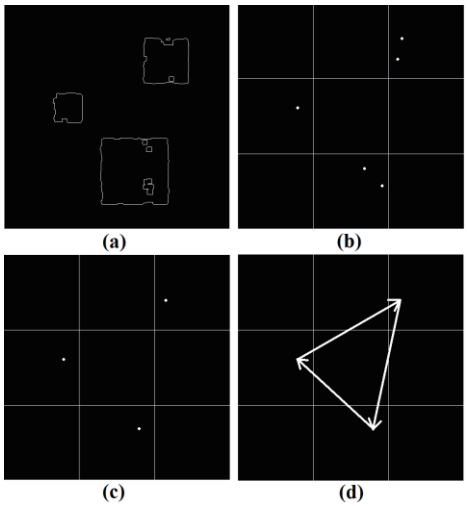

Fig. 5. Preprocess of raw images. (a) The contours of the patterns. (b) The centroids of patterns. (c) The remained centroids. (d) The convex polygon.

$$\mu = \frac{1}{n}\sum_{i=1}^{n} z_i,$$

n represents the number of feature-pixels in target separated area. C_t is a $d \times d$ real positive definite symmetric matrix. The dimensions of C_t does not correspond with n but decided by dimensions of the eigenvector. Since C_t no longer represents eigen data's quantity and sequence, this method is robust in some degree [10]. After obtaining covariance matrices of different target areas, we calculate the similarity between two covariances by using the method in [11], defined as

$$d(t_i, t_j) = \sqrt{(\mu_{t_i} - \mu_{t_j})(C_{t_i} + C_{t_j})^{-1}(\mu_{t_i} - \mu_{t_j})^{\mathrm{T}}},$$

where $t_i, t_j \in \Psi, i \neq j$, μ_{t_i} and μ_{t_j} are the mean eigenvector of target area i and j, C_{t_i} and C_{t_j} are covariance matrices. The similarity of the two target areas is defined by the distance between two covariance matrices. The smaller the distance is, the more similar the two target areas are, vice versa.

C. Definition of Assessment Function

The assessment function is applied to every possible point after filtering by η. Different from the traditional ways of template matching, geometrical differences and similarities of feature-pixels' distribution are used to evaluate each area's matching possibility instead of the correlation of every point's grayscale value. Assessment function is defined as

$$P(x, y) = \frac{K_3}{\Delta\|\mu\|_1} + \frac{K_4}{D},$$

where

$$D = \frac{1}{n}\sum_{i,j\in\Psi} d(t_i, t_j) \quad i \neq j,$$

$$\Delta\|\mu\|_1 = \|\mu_s\|_1 - \|\mu_t\|_1,$$

μ_s and μ_t represent the μ in the source image and template image. $P(x, y)$ describes the matching possibility of the point (x, y). K_3 and K_4 are weight parameters. Now by calculating P for every possible point among remained areas, the best match with the highest P can be picked out. As shown in Fig. 6, the engraved triangle-shaped pattern is matched with the corresponding area in the optical image.

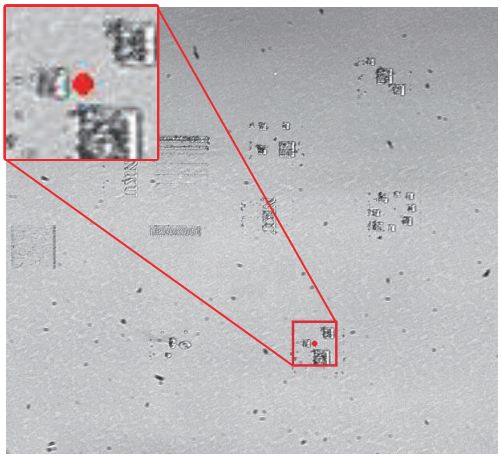

Fig. 6. Matching result of triangle-shaped pattern.

D. Algorithm Flow of the GPTM

In the beginning, initialize parameters: K_1, K_2, K_3, K_4. Then, create a template-size mask, and put it on the upper left corner of the canvas. Slide the mask to traversal all the

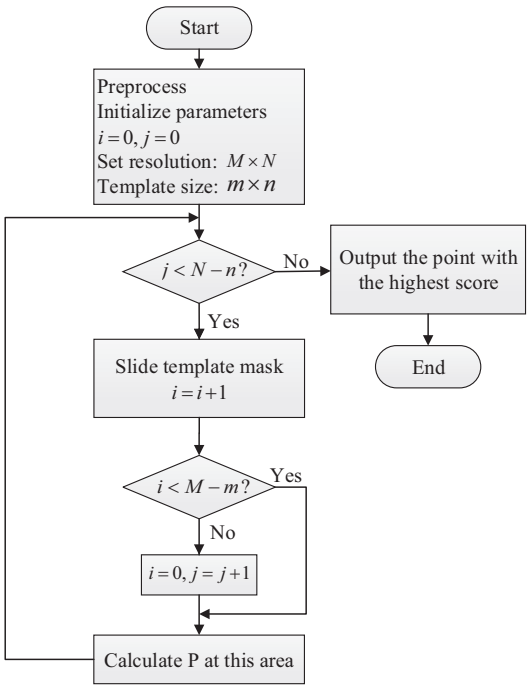

Fig. 7. Flow chart of the GPTM.

interested area on canvas and calculate each pixel's value of assessment function. In the end, output the point with the highest score. The flow chart is shown in Fig. 7.

IV. Experiments

To fully test the performance of the proposed matching algorithm, three more patterns are engraved by the AFM: square, line, ellipse as shown in Fig. 8 to test the algorithm on the new samples, and compare it with the algorithm using the traditional method to further verify the validity of the GPTM.

A. Test on New Patterns

Since GPTM is based on geometrical features, three more patterns: square, line, ellipse are made to test the algorithm's effectiveness. The matching results are shown in Fig. 9 (a), Fig. 9 (b) and Fig. 9 (c). Matching areas are marked with red rectangular. Corresponding with Fig. 8, each pattern is totally located inside the red rectangular, and the centroid point returns the coordinate of the matching position. As the experiment results show, each AFM-scanned template image is precisely matched with the right part of area in source image using a same group of parameters adjusted by using triangle engraved pattern which means to some extent GPTM is robust dealing with different geometrical patterns.

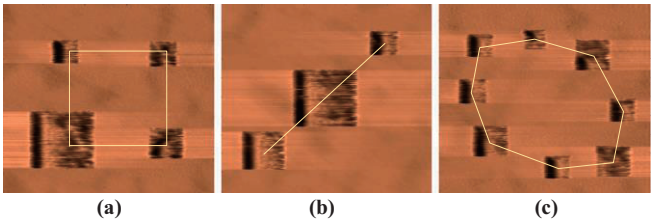

Fig. 8. Three other patterns. (a) Square. (b) Line. (c) Ellipse.

B. Compared with Traditional Method

By comparing the GPTM with the traditional template matching algorithm, the superior matching results by using the GPTM is shown in Fig. 9 (a), Fig. 9 (b) and Fig. 9 (c), and the matching results by using the traditional template matching algorithm is shown in Fig. 9 (d), Fig. 9 (e), Fig. 9 (f). Traditional template matching algorithm uses grayscale correlation of pixels between two areas defined as

$$R(x,y)=\frac{\sum_{x',y'}(T(x',y')\cdot I(x+x',y+y'))}{\sqrt{\sum_{x',y'}T(x',y')^2\cdot\sum_{x',y'}I(x+x',y+y')^2}},$$

where, $T(x, y)$ and $I(x, y)$ are grayscale values of the template image and source image.

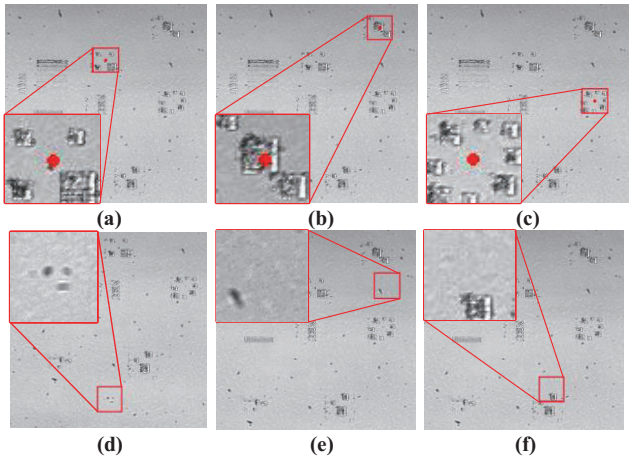

Fig. 9. Matching results. (a) GPTM: square-shaped. (b) GPTM: line-shaped. (c) GPTM: ellipse-shaped. (d) The traditional method: square-shaped. (e) The traditional method: line-shaped. (f) The traditional method: ellipse-shaped.

V. Conclusions

This paper proposes a geometrical patterns based template matching algorithm (GPTM), which is able to successfully match the corresponding target areas between AFM topography images and the reference optical image. In experiments, special samples are made by engraving specific patterns on the petri dish using an AFM. The triangle-shaped sample is used to adjust parameters in the proposed algorithm. Then, the validity and generality of the algorithm are confirmed by applying it to three more patterns: square, line, ellipse. Experiment results show that the three new patterns of AFM-scanned images are successfully matched with the corresponding areas in the optical image accurately, while the traditional template matching algorithm fails. In forthcoming efforts, continuous research interests will be focused on applying the algorithm to more general samples and improving the performance of this algorithm to match the AFM topography images with the reference optical images faster and more accurately.

Acknowledgment

This work is supported by the National Natural Science Foundation of China-Key Program under grant 61633012.

References

[1] J. Pan, H. Zhu, Q. Hou, H. Wang and S. Wang, "Macromolecular and pore structures of Chinese tectonically deformed coal studied by atomic force microscopy," *Fuel*, vol. 139, no. 1, pp. 94-101, 2015.

[2] K. Haase and A. E. Pelling, "Investigating cell mechanics with atomic force microscopy," *Journal of the Royal Society Interface*, vol. 12, no. 104, pp. 1-16, 2015.

[3] Y. F. Dufrêne, "Atomic force microscopy in microbiology: new structural and functional insights into the microbial cell surface," *mBio*, vol. 5, no. 4, pp. 1-14, 2014.

[4] J. N. Sarvaiya, D. S. Patnaik and S. Bombaywala, "Image registration by template matching using normalized cross-correlation," in Proceedings of *2009 International Conference on Advances in Computing, Control, and Telecommunication Technologies*, pp. 819–822, 2009.

[5] L. D. Stefano and S. Mattoccia, "Fast template matching using bounded partial correlation," *Machine Vision and Applications*, vol. 13, no. 4, pp. 213–221, 2003.

[6] H. Torun, O. Finkler and F. L. Degertekin, "Athermalization in atomic force microscope based force spectroscopy using matched microstructure coupling," *Review of Scientific Instruments*, vol. 80, no. 7, pp. 076103, 2009.

[7] S. Belikov and S. Magonov, "Tip-Sample interaction force modeling for AFM simulation, control design, and material property measurement," in Proceedings of *American Control Conference*, pp. 2867-2872, 2011.

[8] A. Sikora and L. Bednarz, "Dynamic speed control in atomic force microscopy to improve imaging time and quality," *Measurement Science and Technology*, vol. 25, no. 4, pp. 1-10, 2014.

[9] Y. Wu, Y. Fang and X. Ren, "A bi-direction asymmetric fast scanning method," in Proceedings of *IEEE International Conference on Manipulation, Manufacturing and Measurement on the Nanoscale*, pp. 171-176, 2015.

[10] X. Zhang, Y. Lv, Y. Miao and D. Yang, "Regional covariance based image superpixels generation," *Computer Science*, vol. 43, no. 5, pp. 318-323, 2016.

[11] L. Karacan, E. Erdem and A. Erdem, "Structure-preserving image smoothing via region covariances," *ACM Transactions on Graphics*, vol. 32, no. 6, pp. 1-11, 2013.